The Irminger Gyre as a key driver of the subpolar North Atlantic overturning on monthly timescales

A. Sanchez-Franks[1], N. P. Holliday[1], D. G. Evans[1], N. Fried[2], O. Tooth[3], L. Chafik[4], Y. Fu[5], F. Li[6], M. F. de Jong[2], and H. L. Johnson[3]

[1]National Oceanography Centre, Southampton, United Kingdom
[2]NIOZ, Royal Netherlands Institute for Sea Research, Texel, Netherlands
[3]Department of Earth Sciences, University of Oxford, Oxford, United Kingdom
[4]Department of Meteorology, Stockholm University, Stockholm, Sweden
[5]School of Earth and Atmospheric Sciences, Georgia Tech, Atlanta, USA
[6]State Key Laboratory of Marine Environmental Science, Xiamen University, Xiamen, China

Key Points:

- The interior Irminger Sea, where the poleward limb of the Irminger Gyre dominates, is a hotspot for the overturning's lower limb variability
- Irminger Gyre transport variability is linked to deep intermediate water masses found in the Irminger Sea on interannual timescales
- Wind stress curl over the Labrador and Irminger Seas drives Irminger Gyre and AMOC variability on monthly timescales

Corresponding author: Alejandra Sanchez-Franks, `alsf@noc.ac.uk`

Abstract

The lower limb of the Atlantic meridional overturning circulation (AMOC) is the equatorward flow of dense waters that have been transformed due to the cooling and freshening of the poleward-flowing upper limb. In the subpolar North Atlantic (SPNA), upper limb variability is primarily set by the North Atlantic Current, whereas lower limb variability is less well understood, particularly at subseasonal timescales. Using observations from a SPNA mooring array, we show that variability of the AMOC's lower limb is connected to poleward flow in the interior Irminger Sea. We identify this flow as the northward branch of the Irminger Gyre (IG), accounting for 55% of the AMOC's lower limb variability on monthly timescales. Further, wind stress curl fluctuations over the Labrador and Irminger Seas drives the IG and AMOC variability on monthly timescales. On interannual timescales, however, increasing thickness of intermediate water within the Irminger Sea coincides with decreasing IG recirculation.

Plain Language Summary

In the subpolar North Atlantic, warm salty waters get transported northwards by the upper branch of the meridional overturning circulation. As they travel northwards, they transform: cooling, densifying and sinking. The cooler deeper waters then get transported back southwards towards the equator in the lower branch of the overturning circulation. The transformation and transport of these waters plays a critical role in our climate system. However, the lower branch of the overturning circulation and the mechanisms controlling how it changes are still not well understood. Observations from a fixed array of moorings between Greenland and Scotland are used here to identify the interior (away from land boundaries) Irminger Sea as a region important for the overturning's lower branch. Specifically, we find that a closed system of currents in the western Irminger Sea, known as the Irminger Gyre, plays an important role in the overturning's variability. The circulation of this gyre is then linked to the recirculation of newly transformed waters that get exported as part of the overturning's lower branch. Finally, we investigate the impact of the atmosphere on Irminger Sea circulation and find that fluctuations of the winds are important drivers of change in this gyre and the overturning.

1 Introduction

The Atlantic meridional overturning circulation (AMOC) is key in regulating the global climate system due to its role in heat and freshwater transport (Srokosz et al., 2012). In the subpolar North Atlantic (SPNA), the light waters of the AMOC's upper limb are densified by water mass transformation and subsequently exported equatorward in the AMOC's lower limb (Brambilla et al., 2008; Desbruyères et al., 2019). The formation and ventilation of dense water within the lower limb also sequesters carbon via the subduction of CO_2-rich surface waters, and thus represents an important carbon sink in the climate system (Sabine et al., 2004; Fontela et al., 2016).

The Overturning in the Subpolar North Atlantic Programme (OSNAP) is a trans-basin ocean observing array that has been providing direct observations of the SPNA AMOC since 2014. The array stretches across the SPNA, spanning Scotland to Greenland (OSNAP East; Fig 1a) and Greenland to Labrador (OSNAP West). One of the key findings of the OSNAP project is that water mass transformation north of OSNAP East dominates the strength and variability of the AMOC in the subpolar North Atlantic compared to OSNAP West (Li et al., 2021; Lozier et al., 2019). This is contrary to previous work that suggested convection in the Labrador Sea sets the variability and strength of the SPNA AMOC (Thornalley et al., 2018; Medhaug et al., 2012). Direct observations have determined that monthly to interannual AMOC variability across OSNAP East is not constrained to a single region but is spread across the western boundary current (i.e., East Greenland Current), as well as the Irminger and Iceland basin (Li et al., 2021). However, satellite and model [hindcast] simulations have shown that the Irminger Sea is a key region for AMOC variability on interannual to decadal time scales (Megann et al., 2021; Chafik et al., 2022).

The Irminger Sea is a climatically important region. At the eastern boundary of the Irminger Sea, the Irminger Current (IC; Fried and de Jong (2022)) transports warm waters northward. As the IC progresses poleward past the OSNAP array, it splits, with one branch continuing northward into the Nordic Seas and the other branch returning southward and eventually joining the cooler fresher waters of the East Greenland Current (EGC) (Pickart et al., 2005). Along the western boundary of the OSNAP East array (Fig. 1a,b), the equatorward flowing EGC advects cool and fresh Arctic-origin waters. In the interior of the Irminger Sea, a narrow cyclonic gyre, known as the Irminger Gyre (IG), circulates in the western side of the basin (Fig. 1a; Våge et al., 2011; Lavender et al., 2000). The IG is largely barotropic and at mid-depths is found to contain Labrador Sea Water (LSW; Våge et al., 2011). The origin of LSW in the Irminger Sea has been traced to local convection (Våge et al., 2011; van Aken et al., 2011) as well as remote formation (i.e. the Labrador Sea) where the IG acts as a highway connecting the Labrador and Irminger Sea (Talley & McCartney, 1982; Straneo et al., 2003; Faure & Speer, 2005). The variability of the IG has been linked to cyclonic wind stress curl off the eastern coast of Greenland (Spall & Pickart, 2003).

While the Irminger Sea has been recently highlighted as an important region for AMOC variability on interannual to decadal timescales (e.g. Megann et al., 2021; Chafik et al., 2022), the connection between the Irminger Sea and the AMOC is unexplored on shorter timescales. Further, several studies have shown buoyancy forcing is an important mechanism for the AMOC on lower frequency timescales (interannual to decadal), but there is a gap in our understanding of driving mechanisms for short time scales (e.g. Jackson et al., 2022). To successfully separate high frequency variability from the longer timescale climate signals we must better understand the drivers of this high frequency variability. Thus, we use direct observations from the OSNAP mooring array to investigate the role of the interior Irminger Sea in the variability of the AMOC on monthly timescales (section 3). We identify the dominant features of the interior Irminger Sea pathways that govern AMOC variability (section 4) and examine the density and atmospheric fields that potentially drive this variability of interior Irminger Sea circulation (sections 5 and 6).

2 Data and Methods

2.1 The OSNAP mooring data

The OSNAP array is constructed from moored temperature, salinity and current meters, autonomous profilers, and hydrographic sections (Li et al., 2017; Lozier et al., 2019).

The velocity and property fields are interpolated onto a regular grid along the OSNAP section using monthly means from 2014 to 2020. The grid has a horizontal and vertical resolution of $\frac{1}{4}^{\circ}$ and 20 m, respectively. The property fields, i.e temperature, salinity and density, are interpolated along the boundaries from the mooring data. In the interior, property fields are estimated in the upper 2000 m via an objective analysis method (further details in Li et al., 2017) using autonomous profilers (i.e. Argo floats and gliders), mooring data, and the WOA 2013 climatology (Locarnini et al., 2013; Zweng et al., 2013). Below 2000 m, in the interior, hydrographic data from research expeditions in 2014 and 2016 are used. Similarly, the velocity field is estimated from mooring velocity data at the boundaries, while in the surface Ekman layer, ERA5 reanalysis wind stress is used (Hersbach et al., 2020), and geostrophic velocities in the interior come from dynamic height (moorings) and altimetry. Further details in Li et al. (2017).

Data from the OSNAP timeseries are compared to absolute dynamic topography (ADT) data from Copernicus Marine Environment Monitoring Service gridded multi-mission satellite altimetry, and wind stress data from ERA5 (Hersbach et al., 2020). Both datasets have a $\frac{1}{4}^{\circ}$ resolution in space and monthly in time.

2.2 Volume transport calculations

In the SPNA, density surfaces slope strongly across the basin. Because of this, the AMOC is measured in terms of density coordinates and can be considered the transformation of light waters associated with the upper limb to denser water transported by the lower limb. Thus, the AMOC is defined here as the maximum of the overturning streamfunction, $\Psi(\sigma, t)$, in density coordinates (Lozier et al., 2019), where v is the volume transport (per unit length in the zonal direction per unit density) perpendicular to the OSNAP array, integrated from west (x_w) to east (x_e) across OSNAP East, and from the surface (σ_{min}) through to all density surfaces:

$$AMOC(t) = max[\Psi(\sigma, t)] = max[\int_{\sigma_{min}}^{\sigma} \int_{x_w}^{x_e} v(x, \sigma, t) dx d\sigma], (Sv) \tag{1}$$

Over the 2014-2020 period, the mean value of the isopycnal of maximum overturning (σ_{MOC}), separating the upper and lower limb, across OSNAP East is 27.57 $kg\ m^{-3}$ (Fig. 1b). The lower limb is defined as the transport component between the sea floor and the time-varying $\sigma_{MOC}(t)$. Throughout the text, all reference to the AMOC and the AMOC lower limb is for OSNAP East only.

3 The interior Irminger Sea and the AMOC's lower limb

The key circulation features of the lower limb are the denser component of the southward flowing EGC, a northwards flow in the western interior Irminger Sea, the overflow waters beneath the northward IC, and the southwards flowing East Reykjanes Ridge Current (ERRC; Fig. 1). An empirical orthogonal function (EOF) analysis of the OSNAP

East velocity field shows that most of the variability across the lower limb is concentrated in the western interior Irminger Sea, and a weaker, secondary region of variability in the IC. The principal component (PC1) time series associated with EOF Mode 1 has a correlation of r = -0.41 (statistically significant at the 95% level) with the AMOC.

The connection between the AMOC and circulation in the Irminger basin is further investigated via the correlation as a function of longitude between the AMOC and the accumulated volume transport integrated from the westernmost point of the OSNAP East array eastward (Fig. 1d). In the region of the EGC, correlation values are r =-0.33 for the accumulated transport and the AMOC lower limb. This weak correlation between the AMOC and the western boundary current on monthly timescales is consistent with findings by Li et al. (2021) who showed that the EGC accounts for only 10% of AMOC variability at OSNAP East. Moving in the eastward direction there is an abrupt increase in correlation within the western and central interior Irminger Sea, a region shown here to be dominated by strong northward flow, with a correlation of up to r = -0.75 and r = -0.67 (statistically significant at the 95% level) for the lower limb and the full water column transport, respectively (Fig. 1d,e). The correlation decreases over the regions of the IC and the ERRC. The low correlation between the AMOC and the boundary currents (i.e. the EGC or IC) may be due to differences in the dominant frequencies of variability associated with the topography of the basin. For example, Hopkins et al. (2019) show that the transport in the boundary currents of the western Irminger Sea varies with a period between 2.5 – 8 days, associated with topographic Rossby waves and/or eddies, whereas further offshore, towards the interior, the dominant periods are longer at $\sim$55 days.

A Hovmöller diagram of the vertically integrated volume transport in the lower limb at each longitudinal grid point across OSNAP East shows a strong and highly variable northward flow in the interior western Irminger Sea (Fig. 1e), coincident with the region of high correlation shown in Figure 1d. The correlation between the AMOC and the time-varying northward flow east of 40°W highlights that an increase in this northward transport coincides with a weakening of the AMOC (Fig. 1e,f). We note that there is no mooring data in the eastern portion of the interior Irminger Sea (Fig. 1b), so geostrophic velocity is calculated from the tall moorings bounding this region. This manifests as a band of lower magnitude variability and lower spatial resolution in this region (Fig. 1e). We also note that after June 2018 a mooring on the western side of the interior Irminger Sea was removed from the array, impacting the estimate of mass transport in that region, and apparent in Fig. 1e (Fu et al., in review), hence for the correlations only the 2014-2018 period is used.

In this section, we have shown that the western interior Irminger Sea is a hotspot of SPNA AMOC variability on monthly timescales, set by the northward flow in this region. The circulation within the western interior Irminger Sea and its connection to the AMOC are further explored in the next section.

4 The cyclonic circulation of the Irminger Sea

The northward transport in the interior Irminger Sea is investigated here via composites of the velocity field and absolute dynamic topography (ADT) during time periods of strong and weak AMOC (Fig. 2). During periods when the AMOC is strong (i.e. greater than one standard deviation above the mean AMOC), there is extremely weak northward transport in the interior Irminger Sea (Fig. 2a). The velocity field also shows a weak bottom-intensified southward velocity core east of 40°W, corresponding to an eastward shift of the deepest core of the Deep Western Boundary Current (Hopkins et al., 2019). Conversely, when the AMOC is weak (i.e. less than one standard deviation below the mean, Fig. 2b), there is a strengthening of the northward flow in the western interior Irminger Sea. Composites of the ADT during strong/weak AMOC periods show a closed cyclonic circulation in the western Irminger Sea. When the AMOC is strong, this gyre expands, and when the AMOC is weak, this gyre contracts (Fig. 2c,d). The ADT across the OSNAP line also shows a steepening of its gradient in the western interior Irminger Sea during the weak AMOC period (Fig. 2e), consistent with the contraction of this gyre and the strengthening of the northwards flow in the interior Irminger Sea, and vice versa. We identify this cyclonic circulation in the western Irminger Sea as the Irminger Gyre (IG), and the northwards flow in the western interior Irminger Sea as its northwards flowing branch.

The northward branch of the cyclonic IG has been previously reported as a weakly baroclinic flow in the mean field (Lavender et al., 2000; Käse et al., 2001; Våge et al., 2011). Here, the IG is a persistent feature east of 40°W and varies strongly with time (Fig. 1e, 2f). The interior Irminger Sea full-depth transport, including the IG and central Irminger interior (Fig. 1d), has a mean northward transport of 14.39 Sv and correlation of r = -0.66 (statistically significant at 95% level) with the monthly AMOC time series over 2014-2018, suggesting that strengthening of the IG transport coincides with a weakening of the AMOC's net southward transport, and vice versa (Fig. 2), consistent with section 3. We also note that the IG's correlation with the AMOC across the full OSNAP array (i.e. OSNAP West and East) increases to r = -0.69. The IG component alone (i.e., 40°W-37.5°W) has an approximate time mean volume transport of 5.5 Sv. This transport is consistent with values previously reported for the northward limb of the IG (i.e. ∼7 Sv; Lavender et al., 2000; Våge et al., 2011; Fried & de Jong, 2022).

The dynamics of the IG are clearly key in setting the variability of the SPNA AMOC, by affecting the strength of the northward flow within the western interior Irminger Sea. In the next section, the Irminger Sea density field is examined as a potential driver of IG variability.

5 The Irminger Gyre and the intermediate water masses of the subpolar North Atlantic

Labrador Sea Water (LSW) is a widespread intermediate water mass in the SPNA, formed within the Labrador and Irminger Seas (Yashayaev et al., 2007; de Jong & de Steur, 2016; Pickart et al., 2003). The density range of LSW is typically 27.7-27.8 $kg\ m^{-3}$ in the Irminger Sea (Holliday et al., 2018) as shown across the lower limb of OSNAP East in Fig. 3.

In the interior Irminger Sea and the IG we observe a potential vorticity (PV) minimum bounded by the 27.7—27.8 $kg\ m^{-3}$ isopycnals (Fig. 3b). PV minima at this depth in the Irminger Sea have been previously used by Pickart et al. (2003) to identify the presence of LSW. Recently, a more detailed description of the water masses in the western Irminger Sea has identified Upper Irminger Sea Intermediate Water (UISIW) and Deep Irminger Sea Intermediate water (DISIW) (Le Bras et al., 2020). UISIW forms near the boundary current with a density range of 27.65-27.73 $kg\ m^{-3}$. DISIW is formed in the interior (around 40°W) with a density range of 27.73-27.77 $kg\ m^{-3}$ and is associated with a local salinity and PV minimum. Temperature-salinity (T-S) profiles within the western interior Irminger Sea highlight a salinity minimum of ∼35.02 $g\ kg^{-1}$ with a mean temperature of ∼3.4 °C along the 27.74 $kg\ m^{-3}$ isopycnal (Fig. 3c), consistent with the DISIW. The T-S properties show that the low PV DISIW is present where we observe the northwards velocity of the IG (Fig. 3c).

Over the OSNAP period, the density and PV structure show a significant increase in volume of the DISIW over time (Fig. 3d,e,f), primarily through the shoaling of the

27.74 $kg\ m^{-3}$ isopycnal (Fig. 3d). The layer thickness between the 27.74 and 27.8 $kg\ m^{-3}$ isopycnal increases by 480 m over 6 years (Fig. 3f). The increase in the deep intermediate water mass suggests that the OSNAP data capture a period of enhanced convection, consistent with de Jong and de Steur (2016). We observe a concurrent decrease in the IG transport over the same period, with a reduction of 4 Sv over 6 years. This is consistent with the hypothesis of Våge et al. (2011) where an increase in volume of intermediate water masses in the interior Irminger Sea causes a decrease in IG velocity on interannual timescales. Fried and de Jong (2022) also found that changes in the gradient of the density field across the Irminger Sea contribute to transport variability in this region (e.g. increases in the density gradient result in higher volume transport). Note that we find no statistically significant trend in the monthly AMOC time series over 2014-2020 or statistically significant correlation between the LSW layer thickness in the Irminger Sea and the AMOC on monthly timescales (not shown).

In this section, we examined the density field as a potential driver of IG variability and found a connection between the IG and the intermediate water masses on low frequency (> monthly) timescales. Next, we examine whether atmospheric forcing provides a mechanistic explanation for the correlation between the northward transport of the IG and AMOC variability on monthly timescales.

6 Atmospheric drivers of the Irminger Gyre and AMOC variability

In the subpolar gyre, strong westerly winds and increased frequency of westerly Greenland tip jets (Våge et al., 2009) are characteristic of positive North Atlantic Oscillation (NAO) conditions (Rogers, 1990). Over the 2014-2018 OSNAP period, NAO positive conditions persisted over the subpolar North Atlantic. During this period, deep convection occurred within the Labrador Sea, south of Cape Farewell and in the Irminger Sea (Piron et al., 2017; de Jong & de Steur, 2016; de Jong et al., 2018). This convection was coincident with regions of positive wind stress curl (WSC) (Fig. 4a). Strong westerlies dominate the subpolar North Atlantic while northeasterlies affect the eastern coast of Greenland (Fig. 4a). We observe positive WSC across most of the Labrador Sea and the eastern subpolar gyre, and negative WSC across the eastern North Atlantic south of 56°N.

A comparison between the OSNAP-derived IG transport and the WSC in the SPNA reveals a region of strong positive correlation (maximum value of r = 0.62 in the Irminger Sea, statistically significant at 95% level) over the Labrador and Irminger Seas (Fig. 4b), in regions where the time-mean WSC is positive (Fig. 4a). This suggests that an increase in the WSC over the Labrador and Irminger Seas leads to a strengthening of IG transport, and vice versa. In general, strong WSC over the Labrador and Irminger Seas acts to spin up the interior circulation, thus connecting the IG and the Labrador Sea (e.g. Lavender et al., 2000; Faure & Speer, 2005). Spall and Pickart (2003) have previously shown that local WSC off Greenland is the main driver of gyre variability in this region on interannual to decadal timescales. Here, we find that WSC over the Labrador and Irminger Seas also drives IG variability, as calculated from OSNAP data, on monthly timescales.

Conversely, the pattern of correlation between the AMOC and WSC across the SPNA shows negative values over the Labrador and Irminger Seas (maximum value r = -0.60), suggesting a strengthening of the WSC is linked to a weakening of the AMOC (Fig. 4c). This is consistent with the mechanism suggested in section 4, i.e., where a strengthening IG drives a weaker AMOC. Thus, increased WSC east of Greenland and over the Irminger Sea acts to strengthen the IG, increasing the northward flow within the western interior Irminger Sea. This increased northward flow subsequently decreases the net southward transport of the AMOC. We note that the max correlations between the WSC and the IG or AMOC weaken (r = 0.48, 0.37, respectively) for the full OSNAP period, 2014-2020. We postulate this is because the relationship between WSC and large-scale circulation changes with different phases of the NAO. Thus, here we have determined that fluctuations in WSC play a key role in driving AMOC variability on monthly timescales during a persistent positive NAO event. These results are consistent with previous studies that have suggested that wind forcing is important on intra-annual timescales (e.g. Jackson et al., 2022; Buckley & Marshall, 2016).

7 Summary

In the SPNA, the Irminger Sea has been shown to be a climatically important region and a key driver of variability for the AMOC on interannual to decadal timescales (Chafik et al., 2022; Megann et al., 2021). Observational studies have further found that variability of the AMOC's lower limb is not constrained to a single region within the eastern subpolar gyre, but rather is spread over the western boundary, Irminger and Iceland basin on monthly to interannual timescales (Li et al., 2021).

In this study, we use data from a trans-basin mooring array to show that the Irminger Sea is a key region, or hotspot, of variability for the AMOC's lower limb on monthly timescales. We find that it is the IG that dominates the variability of the AMOC's lower limb with a correlation of r=-0.75 (accounting for over 55% of its variability), where strengthening in the northward limb of the IG coincides with weakening of the AMOC, and vice versa. Fluctuations in Irminger Sea density and local WSC are investigated as drivers of IG variability. We find that IG variability is linked to the presence and recirculation of Irminger Sea intermediate waters (i.e. DISIW), and that IG transport and DISIW are linked on interannual timescales. Further, it is the fluctuations in WSC over the Labrador and Irminger Seas that dominate IG and AMOC variability, where strengthening of the WSC over the Labrador and Irminger Seas drives strengthening in the IG but weakening in the AMOC on monthly timescales. This relationship between the IG-AMOC and WSC was observed during a period of persistent positive NAO, and may not be representative of other forcing regimes.

In brief, we have demonstrated that wind stress is important to the IG-AMOC system on monthly timescales, while buoyancy forcing is more likely to dominate on interannual and longer timescales (Jackson et al., 2022). More data and further investigation is required to understand the relationship between the wind field and the IG-AMOC during NAO neutral or negative periods.

Acknowledgments

The authors were supported by the UK Natural Environment Research Council National Capability programme CLASS (NE/R015953/1), NERC grants UK OSNAP (NE/K010875/1 and NE/K010875/2), UK OSNAP Decade (NE/T00858X/1), SNAPDRAGON (NE/T013494/1 and NE/T013400/1), and by Innovational Research Incentives Scheme of the Netherlands Organisation for Scientific Research (NWO) under grant agreement nos. 016. Vidi.189.130.

8 Open Research

The OSNAP data can be accessed here: https://www.o-snap.org/data-access/ . Absolute dynamic topography from the Copernicus Marine Environment Monitoring Service gridded multimission satellite altimetry can be accessed from http://marine. copernicus.eu (product ID: SEALEVEL_GLO_PHY_L4_REP_OBSERVATIONS_008_047, last access: 10 December 2020).

References

Brambilla, E., Talley, L. D., & Robbins, P. E. (2008). Subpolar mode water in the northeastern atlantic: 2. origin and transformation. *Journal of Geophysical Research: Oceans*, *113*(C4). Retrieved from `https://agupubs.onlinelibrary.wiley.com/doi/abs/10.1029/2006JC004063` doi: https://doi.org/10.1029/2006JC004063

Buckley, M. W., & Marshall, J. (2016). Observations, inferences, and mechanisms of the atlantic meridional overturning circulation: A review. *Reviews of Geophysics*, *54*(1), 5-63. Retrieved from `https://agupubs.onlinelibrary.wiley.com/doi/abs/10.1002/2015RG000493` doi: https://doi.org/10.1002/2015RG000493

Chafik, L., Holliday, N., Bacon, S., & Rossby, T. (2022). Irminger sea is the center of action for subpolar amoc variability. *Geophysical Research Letters*, *49*(17).

de Jong, M. F., & de Steur, L. (2016). Strong winter cooling over the irminger sea in winter 2014–2015, exceptional deep convection, and the emergence of anomalously low sst. *Geophysical Research Letters*, *43*(13), 7106–7113.

de Jong, M. F., Oltmanns, M., Karstensen, J., & de Steur, L. (2018). Deep convection in the irminger sea observed with a dense mooring array. *Oceanography*, *31*(1), 50–59.

Desbruyères, D. G., Mercier, H., Maze, G., & Daniault, N. (2019). Surface predictor of overturning circulation and heat content change in the subpolar north atlantic. *Ocean Science*, *15*(3), 809–817. Retrieved from `https://os.copernicus.org/articles/15/809/2019/` doi: 10.5194/os-15-809-2019

Faure, V., & Speer, K. (2005). Labrador sea water circulation in the northern north atlantic ocean. *Deep Sea Research Part II: Topical Studies in Oceanography*, *52*(3-4), 565–581.

Fontela, M., García-Ibáñez, M. I., Hansell, D. A., Mercier, H., & Pérez, F. F. (2016). Dissolved organic carbon in the north atlantic meridional overturning circulation. *Scientific reports*, *6*(1), 1–9.

Fried, N., & de Jong, M. F. (2022). The role of the irminger current in the irminger sea northward transport variability. *Journal of Geophysical Research: Oceans*, *127*(3), e2021JC018188.

Fu, Y., Lozier, S., Carrilho Bilo, T., Bower, A., Cunningham, S., Cyr, F., . . .

Yashayaev, I. (in review). Seasonality of the meridional overturning circulation in the subpolar north atlantic. *Communications Earth and Environment*.

Hersbach, H., Bell, B., Berrisford, P., Hirahara, S., Horányi, A., Muñoz-Sabater, J., ... others (2020). The era5 global reanalysis. *Quarterly Journal of the Royal Meteorological Society*, *146*(730), 1999–2049.

Holliday, N. P., Bacon, S., Cunningham, S., Gary, S., Karstensen, J., King, B., ... Mcdonagh, E. (2018). Subpolar north atlantic overturning and gyre-scale circulation in the summers of 2014 and 2016. *Journal of Geophysical Research: Oceans*, *123*(7), 4538–4559.

Hopkins, J., Holliday, N., Rayner, D., Houpert, L., Le Bras, I., Straneo, F., ... Bacon, S. (2019). Transport variability of the irminger sea deep western boundary current from a mooring array. *Journal of Geophysical Research: Oceans*, *124*(5), 3246–3278.

Jackson, L. C., Biastoch, A., Buckley, M. W., Desbruyères, D. G., Frajka-Williams, E., Moat, B., & Robson, J. (2022). The evolution of the north atlantic meridional overturning circulation since 1980. *Nature Reviews Earth & Environment*, *3*(4), 241–254.

Käse, R. H., Biastoch, A., & Stammer, D. (2001). On the mid-depth circulation in the labrador and irminger seas. *Geophysical research letters*, *28*(18), 3433–3436.

Lavender, K. L., Davis, R. E., & Owens, W. B. (2000). Mid-depth recirculation observed in the interior labrador and irminger seas by direct velocity measurements. *Nature*, *407*(6800), 66–69.

Le Bras, I.-A., Straneo, F., Holte, J., de Jong, M., & Holliday, N. (2020). Rapid export of waters formed by convection near the irminger sea's western boundary. *Geophysical Research Letters*, *47*(3), e2019GL085989.

Li, F., Lozier, M. S., Bacon, S., Bower, A., Cunningham, S., de Jong, M., ... others (2021). Subpolar north atlantic western boundary density anomalies and the meridional overturning circulation. *Nature communications*, *12*(1), 1–9.

Li, F., Lozier, M. S., & Johns, W. E. (2017). Calculating the meridional volume, heat, and freshwater transports from an observing system in the subpolar north atlantic: Observing system simulation experiment. *Journal of Atmospheric and Oceanic Technology*, *34*(7), 1483–1500.

Locarnini, R., Mishonov, A., Antonov, J., Boyer, T., Garcia, H., Baranova, O., ... Johnson, D. (2013). Coauthors, 2013: Temperature. vol. 1, world ocean atlas 2013, noaa atlas nesdis 73, 40 pp.

Lozier, M. S., Li, F., Bacon, S., Bahr, F., Bower, A. S., Cunningham, S., ... others (2019). A sea change in our view of overturning in the subpolar north atlantic. *Science*, *363*(6426), 516–521.

Medhaug, I., Langehaug, H. R., Eldevik, T., Furevik, T., & Bentsen, M. (2012). Mechanisms for decadal scale variability in a simulated atlantic meridional overturning circulation. *Climate dynamics*, *39*(1), 77–93.

Megann, A., Blaker, A., Josey, S., New, A., & Sinha, B. (2021). Mechanisms for late 20th and early 21st century decadal amoc variability. *Journal of Geophysical Research: Oceans*, *126*(12), e2021JC017865.

Pickart, R. S., Straneo, F., & Moore, G. K. (2003). Is labrador sea water formed in the irminger basin? *Deep Sea Research Part I: Oceanographic Research Papers*, *50*(1), 23–52.

Pickart, R. S., Torres, D. J., & Fratantoni, P. S. (2005). The east greenland spill jet. *Journal of Physical Oceanography*, *35*(6), 1037–1053.

Piron, A., Thierry, V., Mercier, H., & Caniaux, G. (2017). Gyre-scale deep convection in the subpolar north atlantic ocean during winter 2014–2015. *Geophysical Research Letters*, *44*(3), 1439–1447.

Rogers, J. C. (1990). Patterns of low-frequency monthly sea level pressure variability (1899–1986) and associated wave cyclone frequencies. *Journal of Climate*, *3*(12), 1364–1379.

Sabine, C. L., Feely, R. A., Gruber, N., Key, R. M., Lee, K., Bullister, J. L., ... others (2004). The oceanic sink for anthropogenic co2. *science*, *305*(5682), 367–371.

Spall, M. A., & Pickart, R. S. (2003). Wind-driven recirculations and exchange in the labrador and irminger seas. *Journal of Physical Oceanography*, *33*(8), 1829–1845.

Srokosz, M., Baringer, M., Bryden, H., Cunningham, S., Delworth, T., Lozier, S., ... Sutton, R. (2012). Past, present, and future changes in the atlantic meridional overturning circulation. *Bulletin of the American Meteorological Society*, *93*(11), 1663–1676.

Straneo, F., Pickart, R. S., & Lavender, K. (2003). Spreading of labrador sea water: an advective-diffusive study based on lagrangian data. *Deep Sea Research Part I: Oceanographic Research Papers*, *50*(6), 701–719.

Talley, L. D., & McCartney, M. S. (1982). Distribution and circulation of labrador sea water. *Journal of Physical Oceanography*, *12*(11), 1189–1205.

Thornalley, D. J., Oppo, D. W., Ortega, P., Robson, J. I., Brierley, C. M., Davis, R., ... others (2018). Anomalously weak labrador sea convection and atlantic overturning during the past 150 years. *Nature*, *556*(7700), 227–230.

Våge, K., Pickart, R. S., Sarafanov, A., Knutsen, Ø., Mercier, H., Lherminier, P., ... Bacon, S. (2011). The irminger gyre: Circulation, convection, and interannual variability. *Deep Sea Research Part I: Oceanographic Research Papers*, *58*(5), 590–614.

Våge, K., Spengler, T., Davies, H. C., & Pickart, R. S. (2009). Multi-event analysis of the westerly greenland tip jet based upon 45 winters in era-40. *Quarterly Journal of the Royal Meteorological Society: A journal of the atmospheric sciences, applied meteorology and physical oceanography*, *135*(645), 1999–2011.

van Aken, H. M., de Jong, M. F., & Yashayaev, I. (2011). Decadal and multi-decadal variability of labrador sea water in the north-western north atlantic ocean derived from tracer distributions: Heat budget, ventilation, and advection. *Deep Sea Research Part I: Oceanographic Research Papers*, *58*(5), 505-523. doi: https://doi.org/10.1016/j.dsr.2011.02.008

Yashayaev, I., Bersch, M., & van Aken, H. M. (2007). Spreading of the labrador sea water to the irminger and iceland basins. *Geophysical Research Letters*, *34*(10).

Zweng, M., et al. (2013). World ocean atlas 2013, salinity, noaa atlas nesdis 74, vol. 2, edited by s. *Levitus and A. Mishonov*.

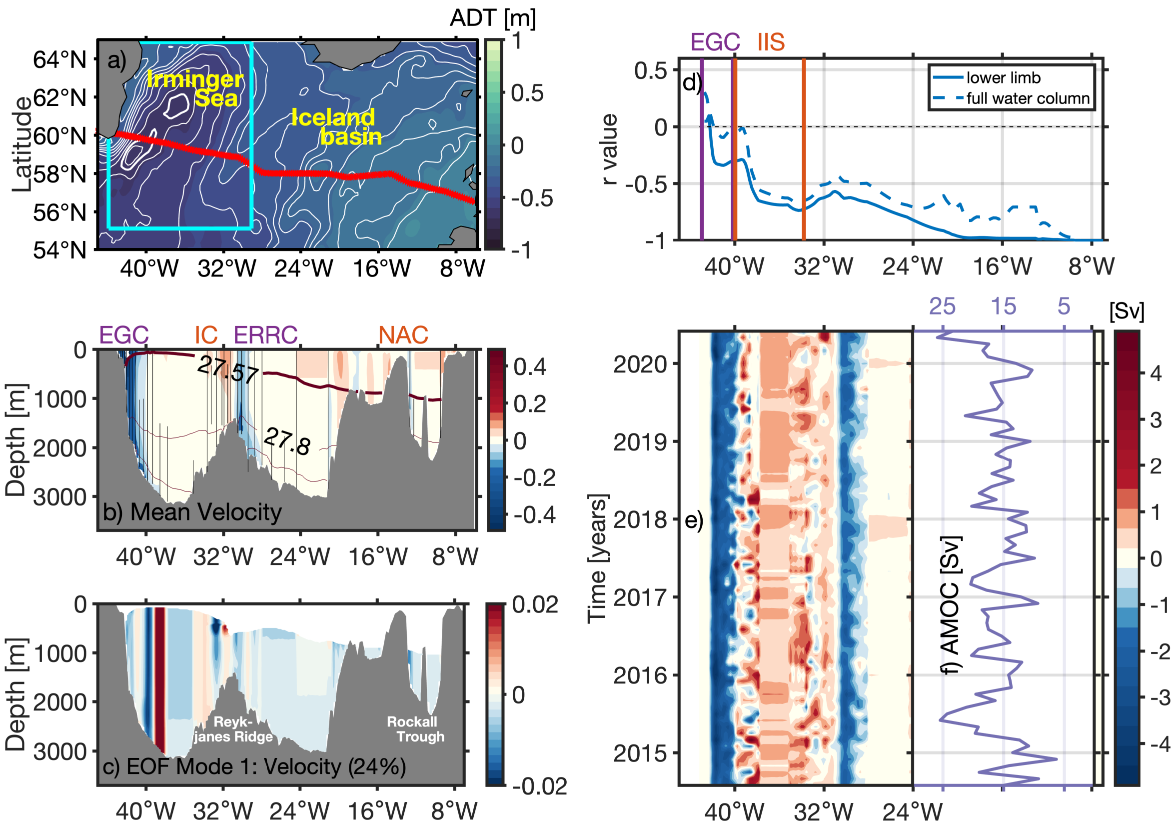

Figure 1. (a) Absolute Dynamic Topography (ADT [m]) over the eastern subpolar gyre. Red line indicates the location of the OSNAP East array. (b) Mean velocity field across OSNAP East. Isopycnals contoured in black, with mean isopycnal of maximum overturning (27.57 $kg\ m^{-3}$) in bold. Vertical black lines indicate mooring locations. (c) EOF mode 1 of velocity variations in the lower limb across OSNAP East. (d) Correlation between the AMOC and the volume transport accumulated eastward along OSNAP East at each longitude. (e) Hovmoller diagram of the vertically integrated volume transport of the lower limb across OSNAP East, with the time series of the AMOC embedded (f) for comparison. In July 2018, a mooring was removed from the interior western Irminger Sea, apparent in panel (e); hence for (b)-(d) only the 2014-2018 OSNAP period were used. EGC = East Greenland Current, IC = Irminger Current, ERRC = East Reykjanes Ridge Current, NAC = North Atlantic Current, LSW = Labrador Sea Water, NEADW = North East Atlantic Deep Water, DSOW = Denmark Straits Overflow Water, ISOW = Iceland-Scotland Overflow Water. IIS = interior Irminger Sea.

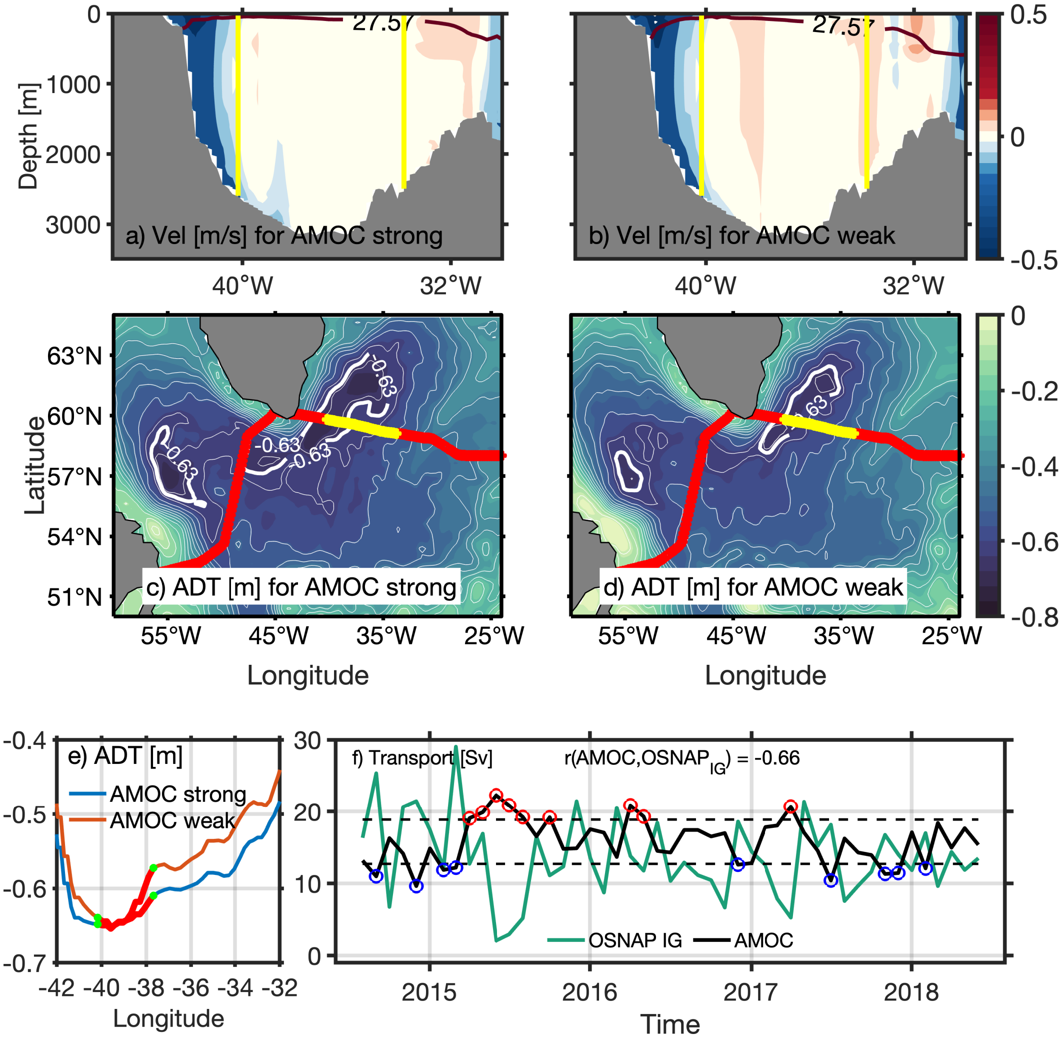

Figure 2. Composites of mean velocity in the interior Irminger Sea during AMOC strong (a) and AMOC weak (b) periods. (c,d) same as in (a,b) but for absolute dynamic topography (ADT) over the SPNA. Red line in (c,d) indicates the location of OSNAP array, while yellow line indicates the span of the interior Irminger Sea, corresponding to yellow lines in (a,b). ADT contours are shown at 0.05 m intervals. (e) ADT over the Irminger Sea along OSNAP line for AMOC strong and weak periods. AMOC strong periods are defined as events one standard deviation above the mean AMOC value, and vice versa. (f) Volume transport of the IG (green line) compared with the AMOC from OSNAP East (black line). Correlation is significant at 99% level.

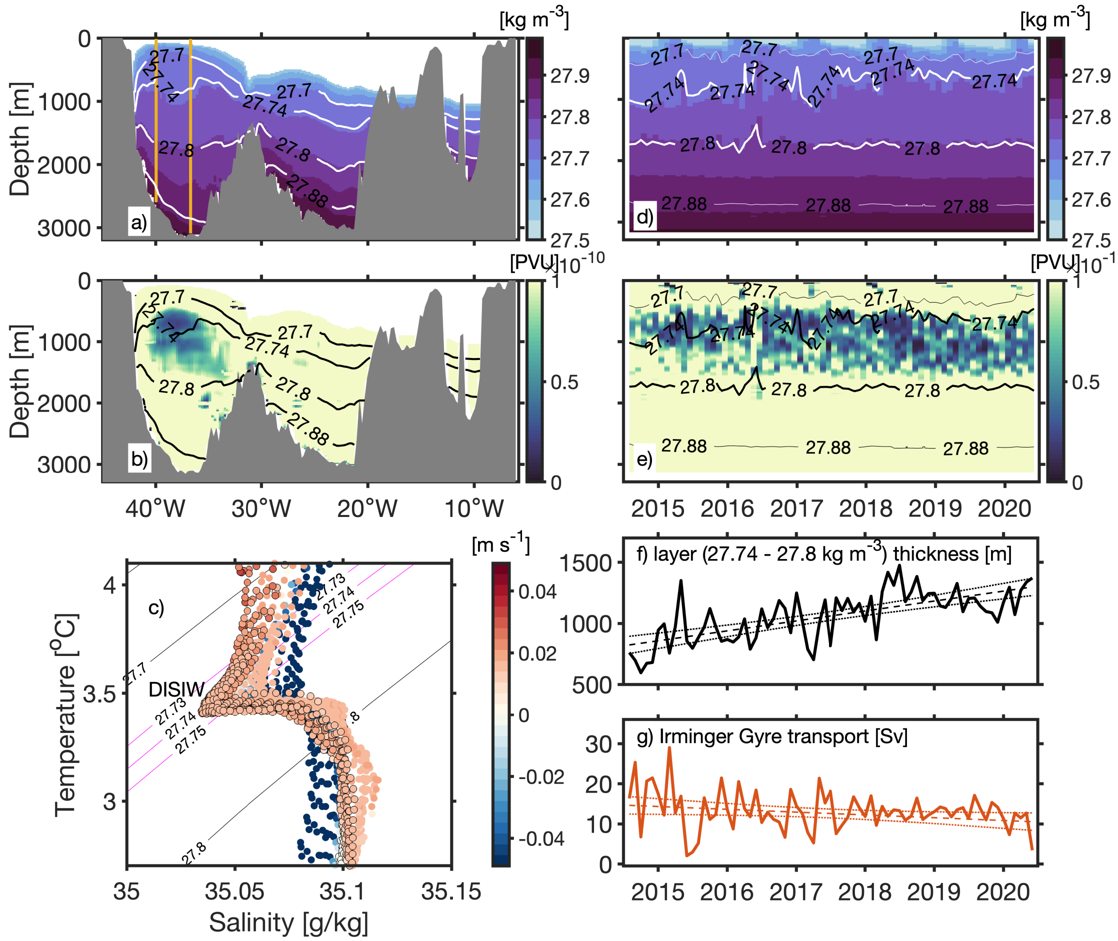

Figure 3. Mean (2014-2020) density (a) and potential vorticity (b) across the lower limb of OSNAP East ($> 27.57\ kg\ m^{-3}$). (c) Conservative temperature and absolute salinity diagram of the time-averaged profiles at every longitude point between the East Greenland coast and the eastern limit of the IG (easternmost yellow line in a); profiles are coloured by velocity ($m\ s^{-1}$) and data points outlined in black indicate profiles from IG region. Temporal evolution of the density (d) and potential vorticity (e) in the zonally averaged IG region (yellow lines in a,b) indicating an increase in lower intermediate waters over time. Time series and trends of the layer (27.4 - 27.8 $kg\ m^{-3}$) thickness (f) and IG transport (g) over OSNAP period. Dotted lines in (f,g) indicate 95% confidence intervals.

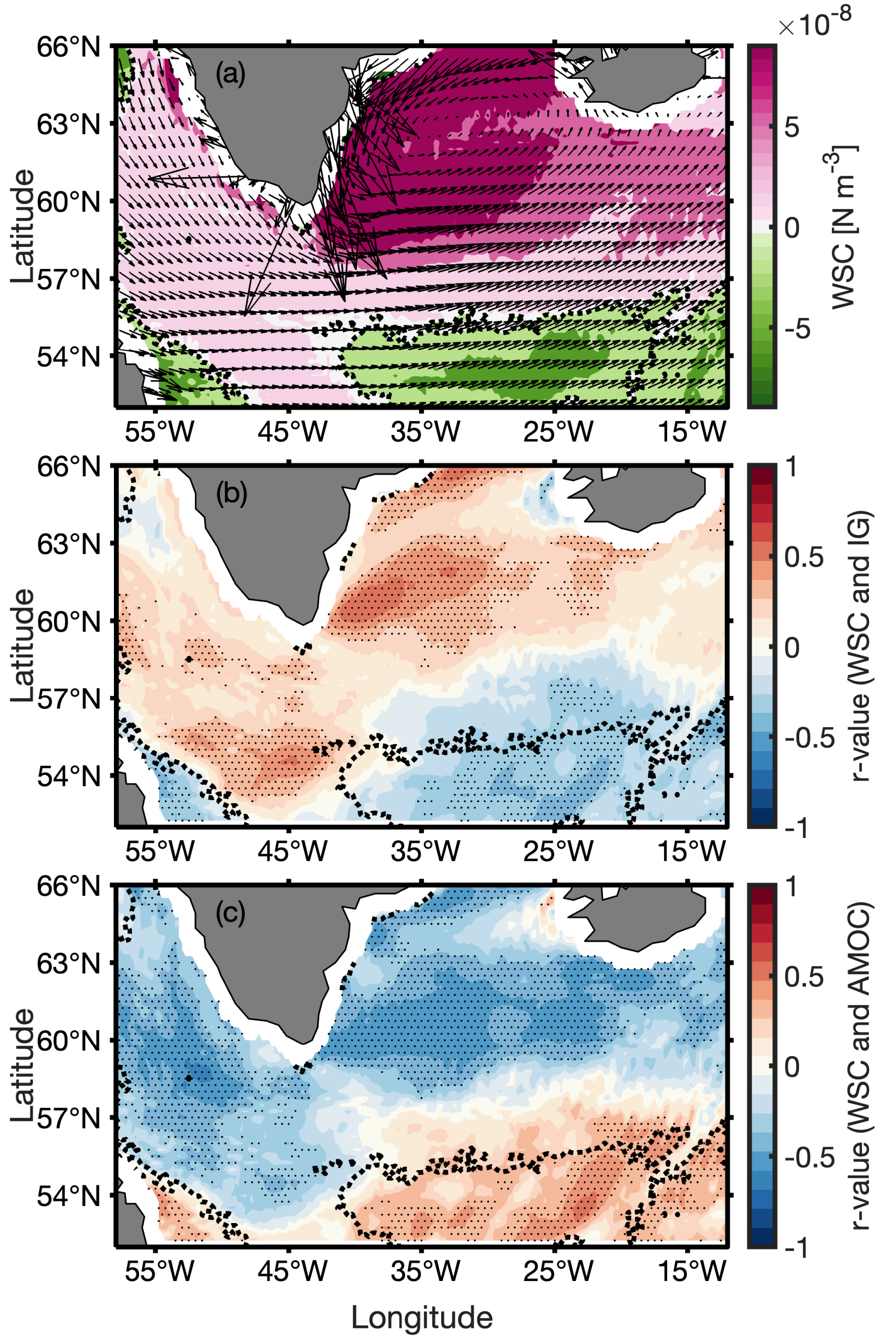

Figure 4. (a) Wind stress (vectors) and wind stress curl (contours) over the 2014-2018 positive North Atlantic Oscillation period (December 2014 to October 2018). Correlation between the wind stress curl and the Irminger Gyre transport at the OSNAP array (b) and the AMOC (c). Black dotted contour (a,b,c) indicates the zero wind stress curl line. Stippling in (b,c) indicates statistical significance at 95% level.

Figure 1.

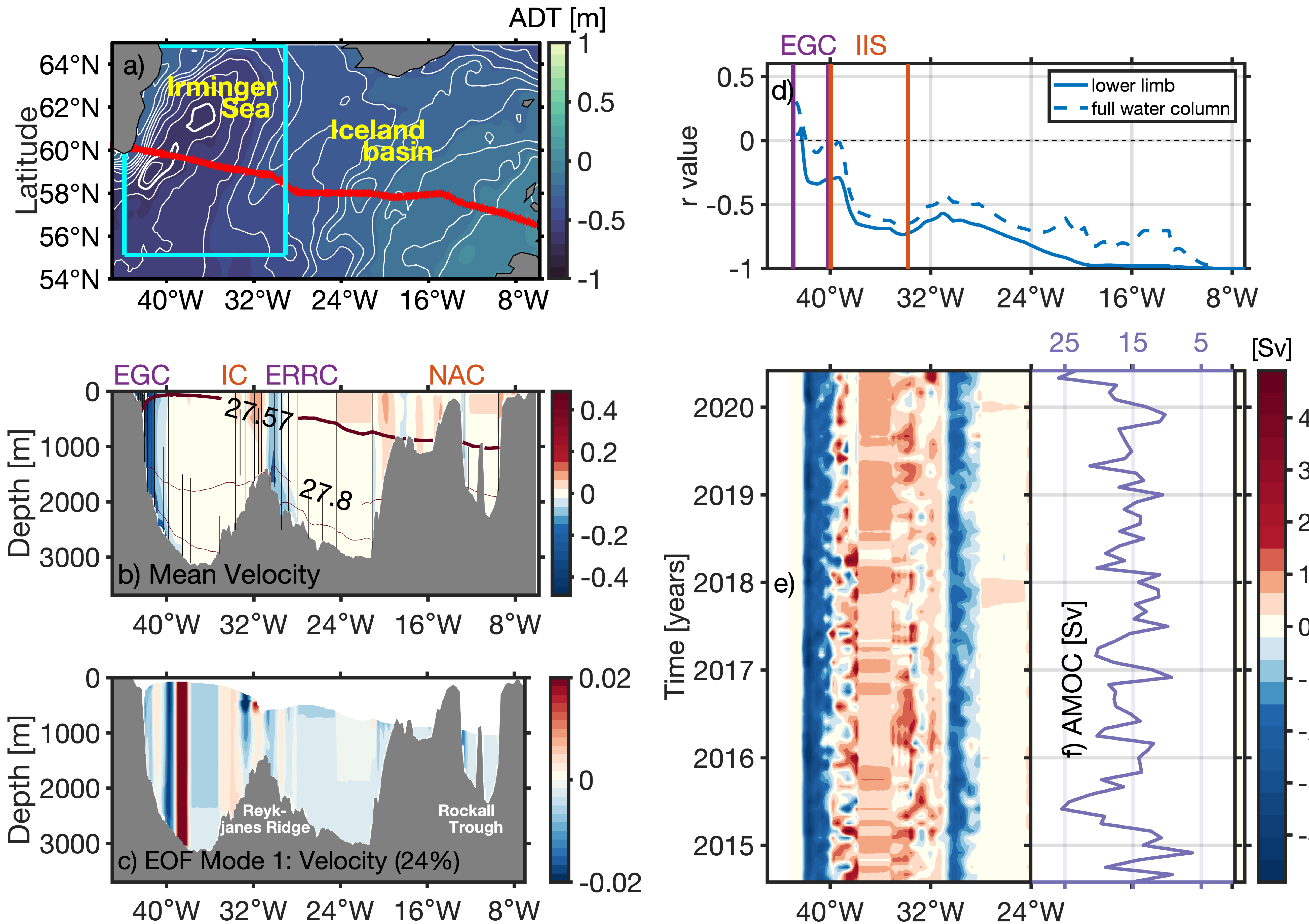

ADT [m]
a)
Irminger Sea
Iceland basin
Latitude
64°N
62°N
60°N
58°N
56°N
54°N
40°W
32°W
24°W
16°W
8°W
1
0.5
0
-0.5
-1
EGC
IIS
d)
lower limb
full water column
r value
0.5
0
-0.5
-1
EGC
IC
ERRC
NAC
27.57
27.8
b) Mean Velocity
Depth [m]
0
1000
2000
3000
0.4
0.2
0
-0.2
-0.4
Reyk-
janes Ridge
Rockall
Trough
c) EOF Mode 1: Velocity (24%)
0.02
0
-0.02
25
15
5
[Sv]
e)
f) AMOC [Sv]
Time [years]
2020
2019
2018
2017
2016
2015
4
3
2
1
0
-1
-2
-3
-4

Figure 2.

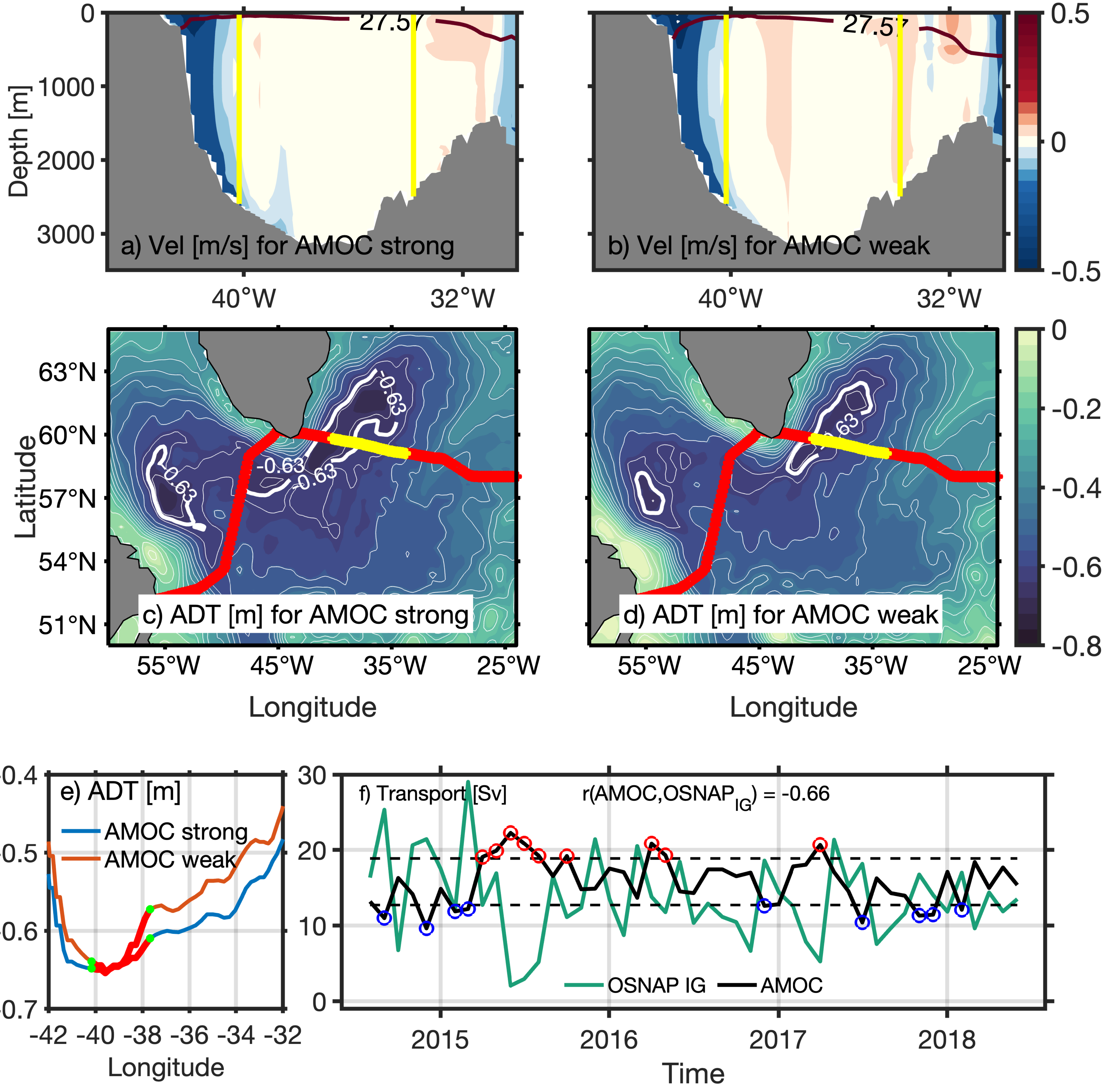

a) Vel [m/s] for AMOC strong
b) Vel [m/s] for AMOC weak
27.57
Depth [m]
0
1000
2000
3000
40°W
32°W
0.5
0
-0.5
c) ADT [m] for AMOC strong
d) ADT [m] for AMOC weak
-0.63
Latitude
63°N
60°N
57°N
54°N
51°N
55°W
45°W
35°W
25°W
Longitude
-0.2
-0.4
-0.6
-0.8
e) ADT [m]
AMOC strong
AMOC weak
-0.4
-0.5
-0.6
-0.7
-42
-40
-38
-36
-34
-32
Longitude
f) Transport [Sv]
r(AMOC,OSNAP$_{IG}$) = -0.66
30
20
10
0
OSNAP IG
AMOC
2015
2016
2017
2018
Time

Figure 3.

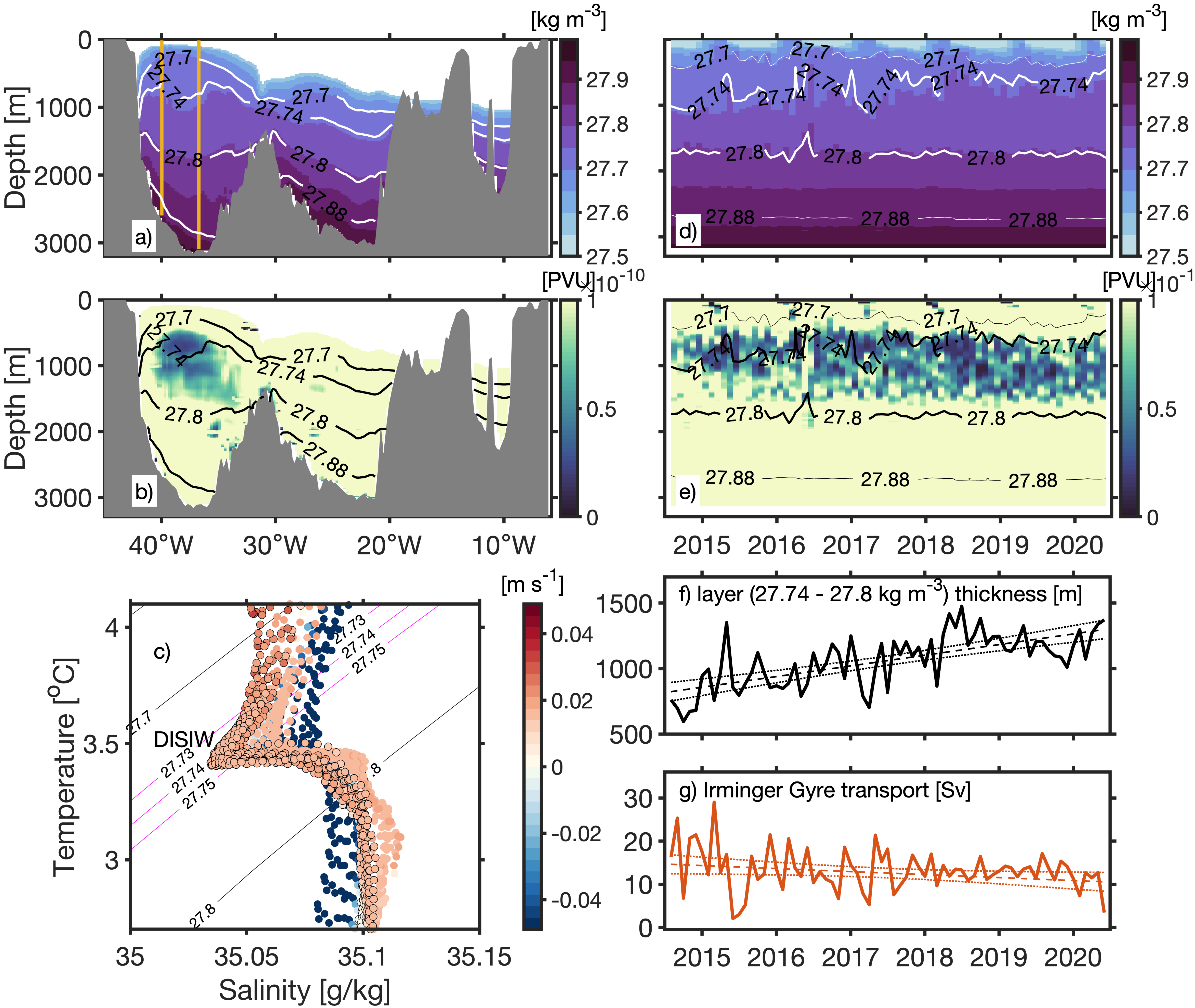

[kg m-3]
Depth [m]
a)
b)
c)
d)
e)
[PVU]
×10-10
40°W
30°W
20°W
10°W
2015
2016
2017
2018
2019
2020
[m s-1]
DISIW
Temperature [°C]
Salinity [g/kg]
f) layer (27.74 - 27.8 kg m-3) thickness [m]
g) Irminger Gyre transport [Sv]

Figure 4.

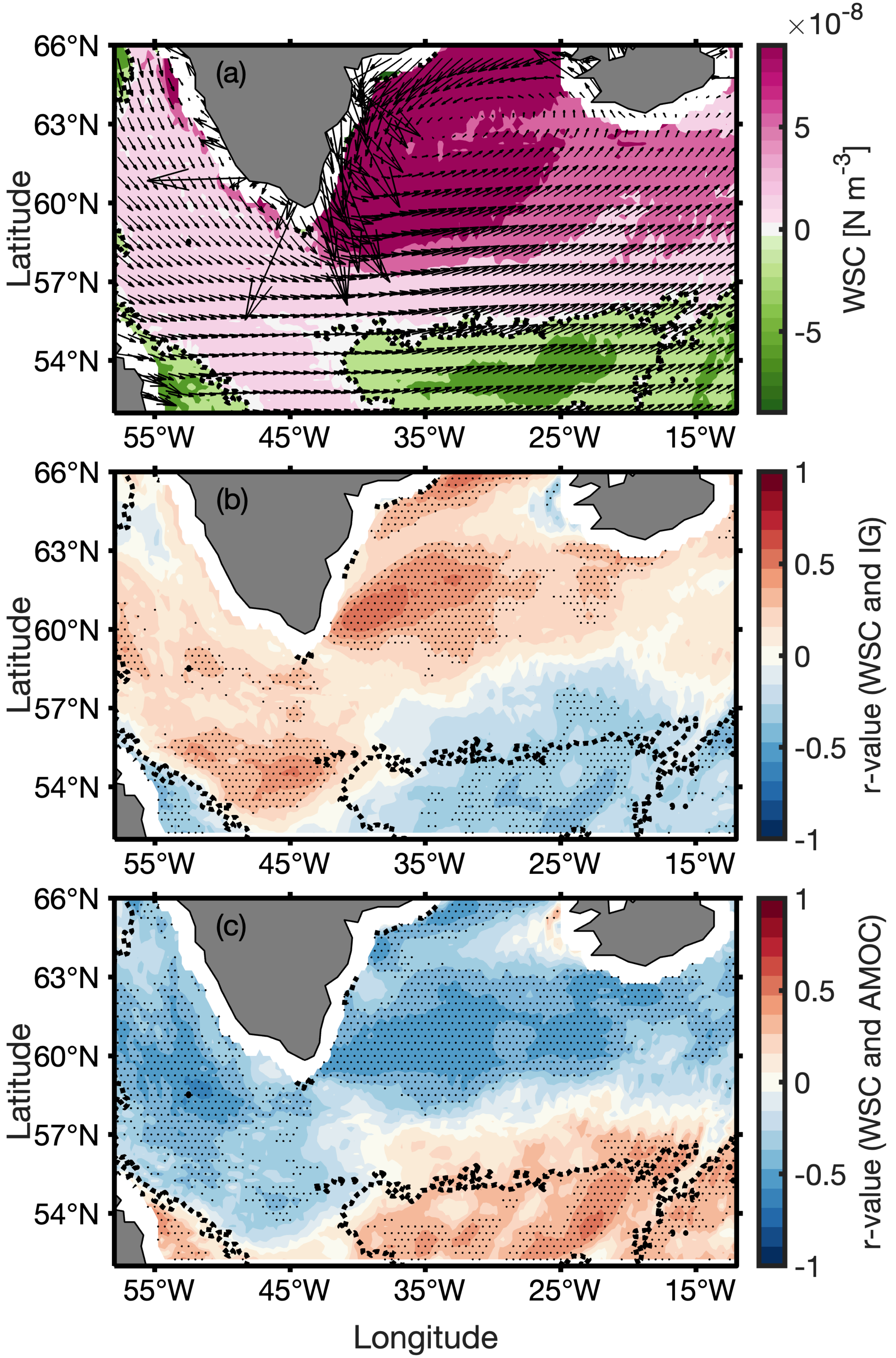

(a)
(b)
(c)
66°N
63°N
60°N
57°N
54°N
55°W
45°W
35°W
25°W
15°W
Latitude
Longitude
×10^-8
WSC [N m^-3]
5
0
-5
r-value (WSC and IG)
r-value (WSC and AMOC)
1
0.5
0
-0.5
-1